2013 IEEE/RSJ International Conference on
Intelligent Robots and Systems (IROS)
November 3-7, 2013. Tokyo, Japan

Passive Dynamic Walking of Rimless Wheel with 2-DOF Wobbling Mass

Fumihiko Asano[1], Takahiro Sogawa[1], Kazuki Tamura[1] and Yukihiro Akutsu[1]

***Abstract*— It was clarified that limit cycle walkers can improve the gait efficiency by using the oscillatory effect of a wobbling mass moving in the body frame. In this research, we investigate the effects of a 2-DOF wobbling mass on the gait properties. As the simplest walker for analysis, we introduce the model of a planar eight-legged rimless wheel (RW) with a passive 2-DOF wobbling mass that is connected to the RW incorporating a spring and a damper. Through numerical simulations, we analyze changes in the gait properties with respect to the system parameters such as the slope angle and the elastic coefficient. Furthermore, entrainment to a wobbling mass motion actively controlled to rotate is also investigated.**

I. INTRODUCTION

The authors have conducted the studies of efficient limit cycle walking of legged robots actively using the dynamic effect of visceral vibration. Through fundamental investigations of simple walkers, it was clarified that improvement of the gait efficiency can be achieved by utilizing the oscillatory effect of passive or active wobbling masses [1][2][3][4]. In the field of robotics [5][6] and other research fields [7][8][9], the importance of internal vibration has been pointed out even though they are differently motivated.

We started the study of legged locomotion with a passive wobbling mass using planar simple walking models composed of rimless wheels (RWs). First, we introduced the model of a passive combined RW (CRW) and examined the effect of the phase difference between the fore and the rear RWs. Through gait analysis, the importance of flattening or smoothing CoM orbit was suggested [10]. After that, we added a passive wobbling mass that vibrates up-and-down to the body frame of the CRW for the purpose of flattening CoM orbit, and confirmed that anti-phase oscillation significantly increases walking speed through numerical simulations and experiments [1]. In the case that the phase difference between the fore and the rear RWs is zero, the body frame always moves parallel to the floor and does not rotate during motion. The wobbling mass therefore vibrates passively up-and-down perpendicular to the floor during walking motion. The speeding-up mechanism can be explained from the viewpoint of a 1-DOF dynamic absorber that cancels out the whole CoM vibration. It is expected that a wobbling motion achieving multiple DOF oscillatory effect would interact more effectively in speeding-up. This subject, however, has not been discussed so far.

[1]F. Asano, T. Sogawa, K. Tamura and Y. Akutsu are with the School of Information Science, Japan Advanced Institute of Science and Technology, 1-1 Asahidai, Nomi, Ishikawa 923-1292, Japan {fasano,sogawa,kzk.tmr.1102,y_akutsu.ibnct.vc}@jaist.ac.jp

Based on the observations, in this paper we investigate the effect of a passive 2-DOF wobbling mass that swings and pumps on the gait properties of a single RW. We introduce the model of a planar single RW with a 2-DOF wobbling mass as the simplest walker for analysis. As is further known in the art, a passive-dynamic gait of a RW is always asymptotically stable and 1-period [11][12][13]. Via dynamical interaction with the wobbling mass, however, curious walking gaits would be generated. Through numerical simulations, we clarify the fundamental gait properties according to the changes in the system parameters such as impedance and slope angle. Furthermore, we examine the effect of a 2-DOF wobbling mass actively controlled to rotate by the joint torque. Through numerical analysis, we show that the walking motion of the RW is entrained to the rhythm of the wobbling mass where the desired wobble frequency is sufficiently high.

II. MODELING

A. Equation of Motion

Fig. 1 shows the model of a planar eight-legged rimless wheel with a passive 2-DOF wobbling mass. Let θ_1 be the angular position of the stance leg with respect to vertical. Let (x, z) be the end-point position of the stance leg. Let L_1 [m] be the leg length or the wheel radius. A passive wobbling mass as a variable length pendulum is connected to the RW incorporating a spring and a damper. Let L_2 [m] be the variable length and θ_2 [rad] be the angular position with respect to vertical.

We assume the followings.

- The end-point of the stance leg is always in contact with the ground without sliding.
- The rotational joint between the RW and the wobbling mass does not generate friction.

Let $\boldsymbol{q} = \begin{bmatrix} x & z & \theta_1 & \theta_2 & L_2 \end{bmatrix}^{\mathrm{T}}$ be the generalized coordinate vector. The equation of motion then becomes

$$\boldsymbol{M}(\boldsymbol{q})\ddot{\boldsymbol{q}} + \boldsymbol{h}(\boldsymbol{q}, \dot{\boldsymbol{q}}) = \boldsymbol{S}u + \boldsymbol{J}^{\mathrm{T}}\boldsymbol{\lambda}. \quad (1)$$

The first term of the right-hand side is the viscoelastic force vector and u [N] stands for the viscoelastic force of the wobbling mass and is given by

$$u = -k\,(L_2 - L_0) - c\dot{L}_2, \quad (2)$$

where k [N/m] is the elastic coefficient and c [N·s/m] is the viscosity coefficient. The driving vector $\boldsymbol{S}$ is also defined as

$$\boldsymbol{S} = \begin{bmatrix} 0 & 0 & 0 & 0 & 1 \end{bmatrix}^{\mathrm{T}}.$$

L_0 [m] is the natural length in the case that L_2 is the total length of the spring. The second term of the right-

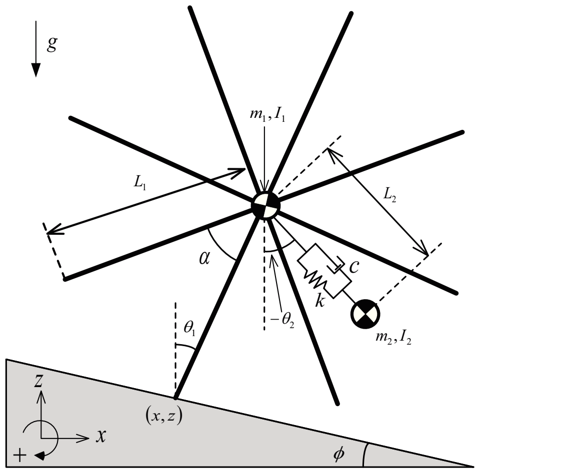

Fig. 1. Model of passive rimless wheel with 2-DOF passive wobbling mass

hand side in Eq. (1) denotes the holonomic constraint force vector which represents the ground reaction forces. The constraint conditions of velocities for ground contact are given by $\dot{x} = 0$ and $\dot{z} = 0$. By summarizing these equations, the Jacobian matrix, $\boldsymbol{J} \in \mathbb{R}^{2\times 5}$, and holonomic constraint condition become

$$\boldsymbol{J}\dot{\boldsymbol{q}} = \begin{bmatrix} 1 & 0 & 0 & 0 & 0 \\ 0 & 1 & 0 & 0 & 0 \end{bmatrix} \dot{\boldsymbol{q}} = \boldsymbol{0}_{2\times 1}. \tag{3}$$

By differentiating Eq. (3) with respect to time, we get $\boldsymbol{J}\ddot{\boldsymbol{q}} = \boldsymbol{0}_{2\times 1}$. The Lagrange undetermined multiplyer vector, $\boldsymbol{\lambda} \in \mathbb{R}^2$, is then solved as

$$\boldsymbol{\lambda} = -\left(\boldsymbol{J}\boldsymbol{M}(\boldsymbol{q})^{-1}\boldsymbol{J}^{\mathrm{T}}\right)^{-1}\boldsymbol{J}\boldsymbol{M}(\boldsymbol{q})^{-1}\left(\boldsymbol{S}u - \boldsymbol{h}(\boldsymbol{q},\dot{\boldsymbol{q}})\right). \tag{4}$$

The second element of $\boldsymbol{\lambda}$, λ_2, is the vertical ground reaction force and must be always positive for stable gait generation. The details of the left-hand terms in Eq. (1) are as follows.

$$\boldsymbol{M}(\boldsymbol{q}) = \begin{bmatrix} m_t & 0 & m_t L_1 \cos\theta_1 & -m_2 L_2 \cos\theta_2 & -m_2 \sin\theta_2 \\ & m_t & -m_t L_1 \sin\theta_1 & m_2 L_2 \sin\theta_2 & -m_2 \cos\theta_2 \\ & & I_1 + m_t L_1^2 & M_{34} & M_{35} \\ & & & I_2 + m_t L_2^2 & 0 \\ \text{Sym.} & & & & m_2 \end{bmatrix}$$

$$M_{34} = -m_2 L_1 L_2 \cos(\theta_1 - \theta_2)$$

$$M_{35} = m_2 L_1 \sin(\theta_1 - \theta_2)$$

$$\boldsymbol{h}(\boldsymbol{q},\dot{\boldsymbol{q}}) = \begin{bmatrix} -m_t L_1 \dot{\theta}_1^2 \sin\theta_1 + m_2\dot{\theta}_2\left(L_2\dot{\theta}_2\sin\theta_2 - 2\dot{L}_2\cos\theta_2\right) \\ -m_t L_1 \dot{\theta}_1^2 \cos\theta_1 + m_2\dot{\theta}_2\left(L_2\dot{\theta}_2\cos\theta_2 + 2\dot{L}_2\sin\theta_2\right) \\ -L_1\left(2m_2\dot{L}_2\dot{\theta}_2\cos(\theta_1-\theta_2) + m_2 L_2\dot{\theta}_2^2\sin(\theta_1-\theta_2)\right) \\ m_2 L_2\left(2\dot{L}_2\dot{\theta}_2 + L_1\dot{\theta}_1^2\sin(\theta_1-\theta_2)\right) \\ -m_2\left(L_2\dot{\theta}_2^2 - L_1\dot{\theta}_1^2\cos(\theta_1-\theta_2)\right) \end{bmatrix} + \begin{bmatrix} 0 \\ m_t g \\ -m_t g L_1 \sin\theta_1 \\ m_2 g L_2 \sin\theta_2 \\ -m_2 g \cos\theta_2 \end{bmatrix}$$

Where $m_t := m_1 + m_2$ [kg] is the robot's total mass.

B. Collision Equations

The collision equation is modeled on the assumption of inelastic collision as follows.

$$\boldsymbol{M}(\boldsymbol{q})\dot{\boldsymbol{q}}^+ = \boldsymbol{M}(\boldsymbol{q})\dot{\boldsymbol{q}}^- + \boldsymbol{J}_I(\boldsymbol{q})^{\mathrm{T}}\boldsymbol{\lambda}_I \tag{5}$$

$$\boldsymbol{J}_I(\boldsymbol{q})\dot{\boldsymbol{q}}^+ = \boldsymbol{0}_{2\times 1} \tag{6}$$

$$\boldsymbol{J}_I(\boldsymbol{q}) = \begin{bmatrix} 1 & 0 & L_1\left(\cos\theta_1^- - \cos(\alpha - \theta_1^-)\right) & 0 & 0 \\ 0 & 1 & -L_1\left(\sin\theta_1^- + \sin(\alpha - \theta_1^-)\right) & 0 & 0 \end{bmatrix} \tag{7}$$

Here, the superscripts "$-$" and "$+$" stand for immediately before and immediately after impact. In Eq. (5), we do not consider the stance-leg exchange and the relation $\boldsymbol{q}^+ = \boldsymbol{q}^- = \boldsymbol{q}$ thus holds. Following Eqs. (5) and (6), the velocity vector immediately after impact can be solved as

$$\dot{\boldsymbol{q}}^+ = \left(\boldsymbol{I}_5 - \boldsymbol{J}_I(\boldsymbol{q})^{\mathrm{T}}\left(\boldsymbol{J}_I(\boldsymbol{q})\boldsymbol{M}(\boldsymbol{q})^{-1}\boldsymbol{J}_I(\boldsymbol{q})^{\mathrm{T}}\right)^{-1}\boldsymbol{J}_I(\boldsymbol{q})\right)\dot{\boldsymbol{q}}^-. \tag{8}$$

The velocities of the end-point of the stance leg must be reset to

$$\dot{x}^+ = 0, \quad \dot{z}^+ = 0.$$

In the positional vector immediately after impact, $\boldsymbol{q}^+$, the angular position must be reset to

$$\theta_1^+ = \theta_1^- - \alpha = \phi - \frac{\alpha}{2}. \tag{9}$$

The end-point position, (x, z), does not concern to the generated motion, so we reset it to $(x^+, z^+) = (0, 0)$ in the numerical simulations.

III. GAIT ANALYSIS

A. Effect of Elasticity

First, we analyze the effect of elastic coefficient, k, by choosing the physical parameters except k as listed in Table I. We conduct numerical simulations according to the following procedure.

Procedure 1: Set k to 0 [N/m] and ϕ to 0.13 [rad].

(1a) Set the initial condition to the following values.

$$\boldsymbol{q}(0) = \begin{bmatrix} 0 & 0 & 0 & 0 & L_0 \end{bmatrix}^{\mathrm{T}}, \quad \dot{\boldsymbol{q}}(0) = \begin{bmatrix} 0 & 0 & 0.5 & 0 & 0 \end{bmatrix}^{\mathrm{T}} \tag{10}$$

(1b) Start passive dynamic walking.

(1c) After 100 [s] of starting, save the gait descriptors for 20 steps.

(1d) Increase k by 2.5 [N/m] and return to (1a).

(1e) Repeat from (1a) to (1d) until $k = 2000$ [N/m].

The walking speed, V [m/s], is defined by the step length, ΔX_g [m], and the step period, T [s], as

$$V = \frac{\Delta X_g}{T}, \quad \Delta X_g = 2L_1 \sin\frac{\alpha}{2}.$$

The frequency of the generated walking gait, f_w [Hz], is also defined as the reciprocal of the step period by

$$f_w = \frac{1}{T}.$$

Since ΔX_g is constant, f_w can be uniquely calculated by V and vice versa. We therefore plot only one of them in the following.

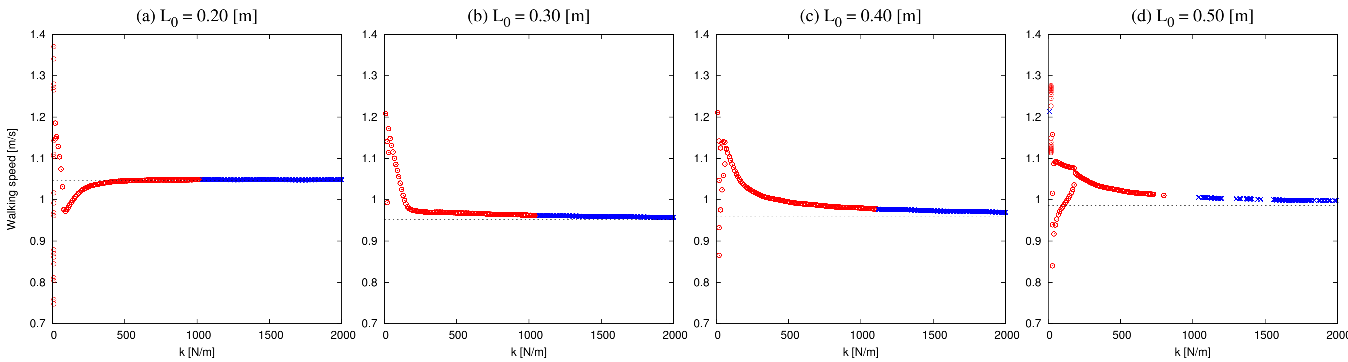

Fig. 2. Walking speed versus elastic coefficient for four values of L_0 where $\phi = 0.13$ [rad] and $c = 10.0$ [N·s/m]

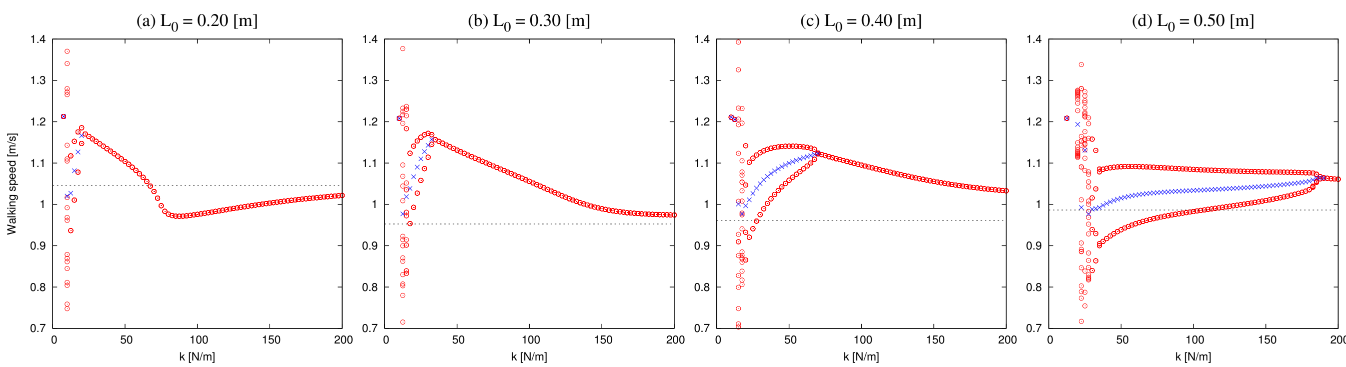

Fig. 3. Magnified view of Figure 2 and average walking speed in 2-period gait

TABLE I

PHYSICAL PARAMETERS

m_1	2.0	kg
m_2	1.0	kg
I_1	0.01	kg·m^2
I_2	0.005	kg·m^2

L_1	1.0	m
α	$\pi/4$	rad
c	10.0	N·s/m

Fig. 2 shows the analysis results of the walking speed for four values of L_0 with respect to k. We plotted the walking speed with red "◯" in the case that the following two conditions are satisfied.

(C1) The vertical ground reaction force is always positive during motion.

(C2) The wobbling mass does not hit the ground during walking.

We also plotted that in the case where (C1) is not satisfied with blue "×" for the purpose of reference. In Fig. 2 (d), however, there are cases neither of "◯" and "×". This is the case that the walker could not overcome the potential barrier at mid-stance or fell backward. In addition, we plotted the walking speed where the prismatic joint of the wobbling mass is mechanically locked with a dotted line.

In the cases except Fig. 2 (a) ($L_0 = 0.20$ [m]), the walking speed becomes higher than the locked case and converges to it as k becomes sufficiently large. Inversely, as k decreases, the walking speed monotonically increases more and bifurcation occurs except the case of $L_0 = 0.20$ [m]. Fig. 3 shows the magnified views of Fig. 2 for $0 \leq k \leq 200$ [N/m]. We also plotted the average value in 2-period gaits with blue "×" for comparison. We can see that, in Fig. 3 (b)(c)(d), the walking speed in 1-period gait monotonically increases with the decrease of k and exhibits period-doubling bifurcation in each case. In Fig. 3 (a), the walking speed decreases but changes to increase later with the decrease of k. In all cases, the average walking speed in 2-period gait monotonically decreases with the decrease of k. We can conclude that the walking speed reaches a local maximum value at the first bifurcation point.

As k decreases further, 1-period gaits with higher walking speed appear after passing chaotic gaits. There might be some changes in the phase relation between the walking gait and the wobbling motion: transition from in-phase to anti-phase oscillation [1].

B. Effect of Slope and Hysteresis

Next, we analyze the effect of the slope on the gait properties. We conduct numerical simulations according to the following procedure.

Procedure 2: Set k to 100 [N/m] and ϕ to 0.10 [rad].

(2a) Set the initial condition to the values of Eq. (10).

(2b) Start passive dynamic walking.

(2c) After 100 [s] of starting, save the gait descriptors for 20 steps.

(2d) Increase ϕ by 0.01 [rad] and return to (2a).

(2e) Repeat from (2a) to (2d) until $\phi = 0.30$ [rad].

Fig. 4 shows the analysis results of the walking speed for four values of L_0 with respect to the slope. In this

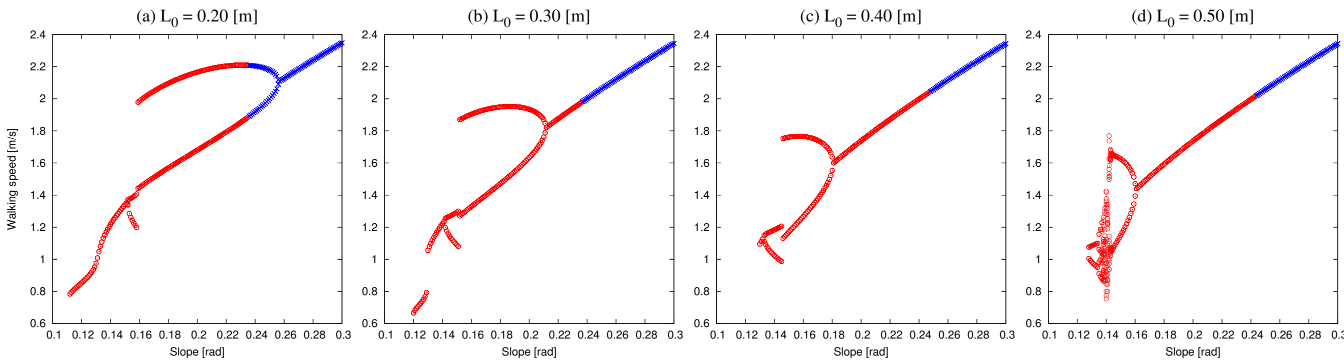

Fig. 4. Walking speed versus slope for four values of L_0 where $k = 100$ [N/m] and $c = 10$ [N·s/m]

case, we also plotted the case where (C1) is not satisfied with blue "×". In each case, we can see that there is a hop phenomenon. In other words, there are two different bifurcation diagrams. Especially in Fig. 4 (d), two chaotic gaits intercross.

To examine it more closely, we re-execute numerical simulations according to the following procedure.

Procedure 3: Set k to 100 [N/m], ϕ to 0.10 (or 0.30) [rad], and the initial condition to the values of Eq. (10).

(3a) Start passive dynamic walking.
(3b) After 100 [s] of starting, save the gait descriptors for 20 steps and the steady state immediately after impact.
(3c) Increase (or decrease) ϕ by 0.01 [rad] and return to (3a).
(3d) Repeat from (3a) to (3c) until $\phi = 0.30$ (or 0.10) [rad].

Fig. 5 shows the analysis results of the walking speed. We can see that hysteresis occurs and there exist two different 2-period gaits where $0.152 \leq \phi \leq 0.160$ [rad]. Fig. 6 shows the simulation results of the steady gait where $\phi = 0.155$ [rad] obtained by increasing ϕ, whereas Fig. 7 shows those obtained by decreasing ϕ. We can determine the distinction between the two generated gaits. From the generated pattern of θ_1 in Fig. 7 (a), we can see that the two steady periods are remarkably different. From that of θ_2 in the same figure, we can see that the wobbling mass moves backward and forward greater than that in Fig. 6 (a). (See our movie)

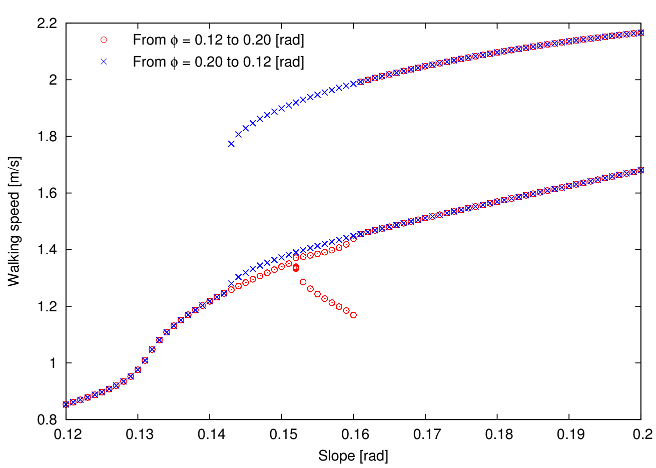

Fig. 5. Hysteresis in walking speed where $L_0 = 0.2$ [m] and $k = 100$ [N/m]

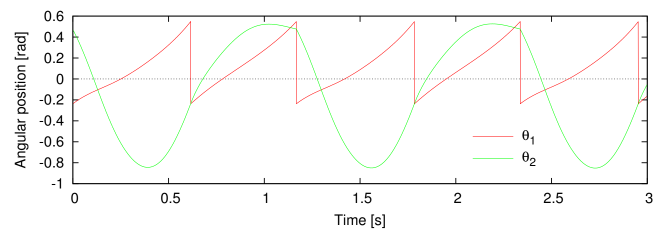

(a) Angular positions, θ_1 and θ_2

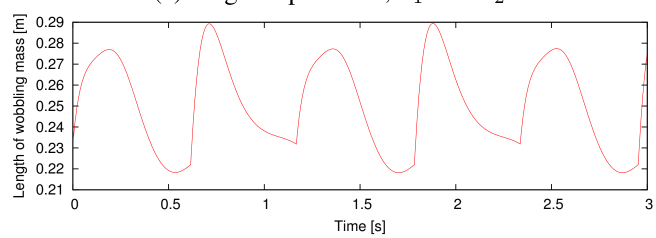

(b) Length of wobbling mass, L_2

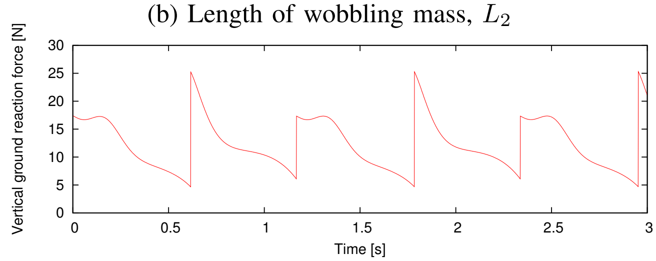

(c) Vertical ground reaction force, λ_2

Fig. 6. Steady 2-period passive-dynamic gait where $L_0 = 0.2$ [m], $k = 100$ [N/m] and $\phi = 0.155$ [rad] obtained by increasing ϕ

Note that the walker has three different eigenmodes: the eigenfrequency of the walking gait (RW), that of swinging motion of the wobbling mass, and that of pumping motion of it. Identifying the dominant mode is, however, not easy because all the variables synchronize each other while intricately interacting. More investigations are necessary.

IV. ACTUATION AND ENTRAINMENT

A. Problem Formulation

In this section, we examine the effect of actuating the 2-DOF wobbling mass on the gait properties. We consider that

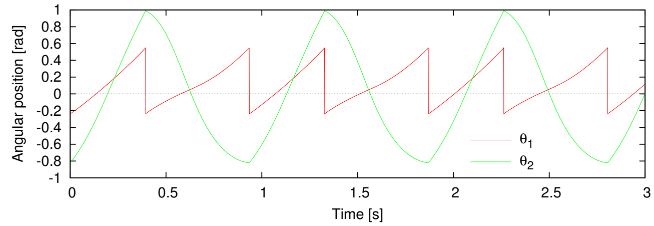

(a) Angular positions, θ_1 and θ_2

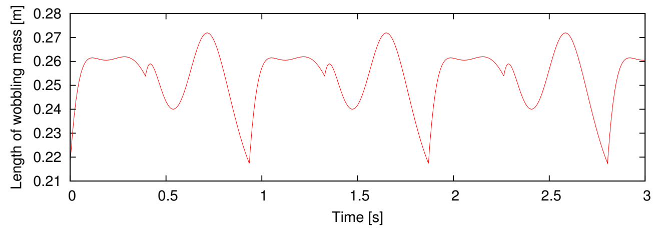

(b) Length of wobbling mass, L_2

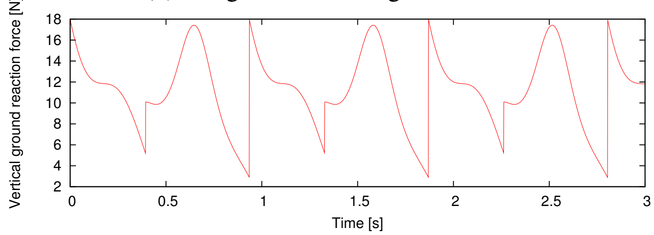

(c) Vertical ground reaction force, λ_2

Fig. 7. Steady 2-period passive-dynamic gait where $L_0 = 0.2$ [m], $k = 100$ [N/m] and $\phi = 0.155$ [rad] obtained by decreasing ϕ

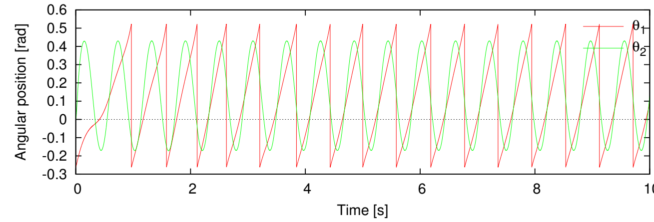

(a) Angular positions, θ_1 and θ_2

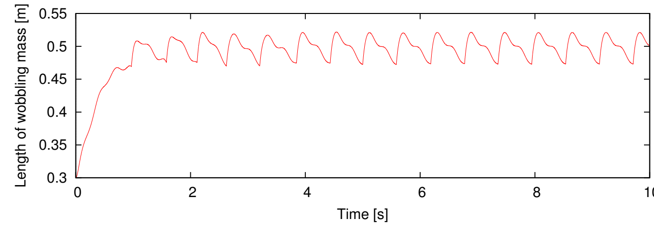

(b) Length of wobbling mass, L_2

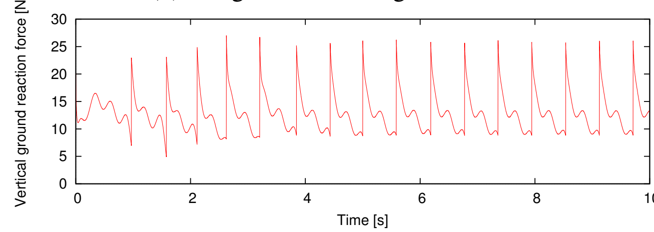

(c) Vertical ground reaction force, λ_2

Fig. 8. Simulation results of passive dynamic walking with active wobbling mass where $L_0 = 0.3$ [m], $\phi = 0.13$ [rad], $A_m = 0.3$ [m] and $f_c = 1.7$ [Hz]

the walker can exert a joint torque, $\hat{u}$, between the RW and the wobbling mass. The equation of motion then becomes

$$\boldsymbol{M}(\boldsymbol{q})\ddot{\boldsymbol{q}} + \boldsymbol{h}(\boldsymbol{q}, \dot{\boldsymbol{q}}) = \boldsymbol{S}u + \hat{\boldsymbol{S}}\hat{u} + \boldsymbol{J}^{\mathrm{T}}\boldsymbol{\lambda}, \tag{11}$$

where $\hat{\boldsymbol{S}} = \begin{bmatrix} 0 & 0 & 1 & -1 & 0 \end{bmatrix}^{\mathrm{T}}$ and the condition for holonomic constraint is the same as Eq. (3). We then apply an output following control for the wobbling mass so that it vibrates centering around normal to the slope. Let θ_2 be the control output. The second order derivative with respect to time becomes $\ddot{\theta}_2 = \boldsymbol{C}\ddot{\boldsymbol{q}} = A(\boldsymbol{q})\hat{u} + B(\boldsymbol{q}, \dot{\boldsymbol{q}})$ where $\boldsymbol{C} = \begin{bmatrix} 0 & 0 & 0 & 1 & 0 \end{bmatrix}^{\mathrm{T}}$ and

$$\begin{aligned} A(\boldsymbol{q}) &= \boldsymbol{C}\boldsymbol{M}(\boldsymbol{q})^{-1}\left(\boldsymbol{I}_5 - \boldsymbol{J}^{\mathrm{T}}\boldsymbol{X}(\boldsymbol{q})^{-1}\boldsymbol{J}\right)\boldsymbol{M}(\boldsymbol{q})^{-1}\hat{\boldsymbol{S}}, \\ B(\boldsymbol{q}, \dot{\boldsymbol{q}}) &= \boldsymbol{C}\boldsymbol{M}(\boldsymbol{q})^{-1}\left(\boldsymbol{I}_5 - \boldsymbol{J}^{\mathrm{T}}\boldsymbol{X}(\boldsymbol{q})^{-1})\boldsymbol{J}\right)\boldsymbol{M}(\boldsymbol{q})^{-1} \\ &\quad \times (\boldsymbol{S}u - \boldsymbol{h}(\boldsymbol{q}, \dot{\boldsymbol{q}})). \end{aligned}$$

The control input, $\hat{u}$, for achieving $\theta_2 \to \theta_{2d}(t)$ can be determined as

$$\begin{aligned} \hat{u} &= A(\boldsymbol{q})^{-1}(v - B(\boldsymbol{q}, \dot{\boldsymbol{q}})), \\ v &= \ddot{\theta}_{2d}(t) + K_D\left(\dot{\theta}_{2d}(t) - \dot{\theta}_2\right) + K_P(\theta_{2d}(t) - \theta_2). \end{aligned}$$

Here, K_P and K_D are PD gains and are positive constants. The desired-time trajectory, $\theta_{2d}(t)$, is also given by

$$\theta_{2d}(t) = A_m \sin(2\pi f_c t),$$

where f_c [Hz] is the desired wobble frequency and A_m [rad] is the desired amplitude.

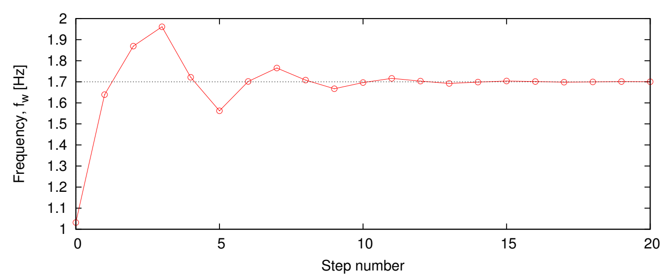

Fig. 9. Evolution of frequency of walking gait

B. Typical Gait

Fig. 8 shows the simulation results of passive dynamic walking on the slope of 0.13 [rad]. The walker started walking from a certain initial condition. The physical parameters are chosen as listed in Table I. The physical and control parameters of the wobbling mass are chosen as $k = 100$ [N/m], $L_0 = 0.30$ [m], $A_m = 0.3$ [rad], and $f_c = 1.7$ [Hz]. The PD gains are also chosen as $K_D = 100$ and $K_P = 2500$. We can see that a stable 1-period gait is generated. Fig. 8 (a) supports that the motion of the generated walking gait and that of the active wobbling mass synchronize each other. In this case, as described later, the walking gait is entrained to the motion of the active wobbling mass as is the case in CRWs [3][4]. Fig. 9 plots the evolution of the frequency, f_w, to confirm it. We can see that f_w converges to f_c.

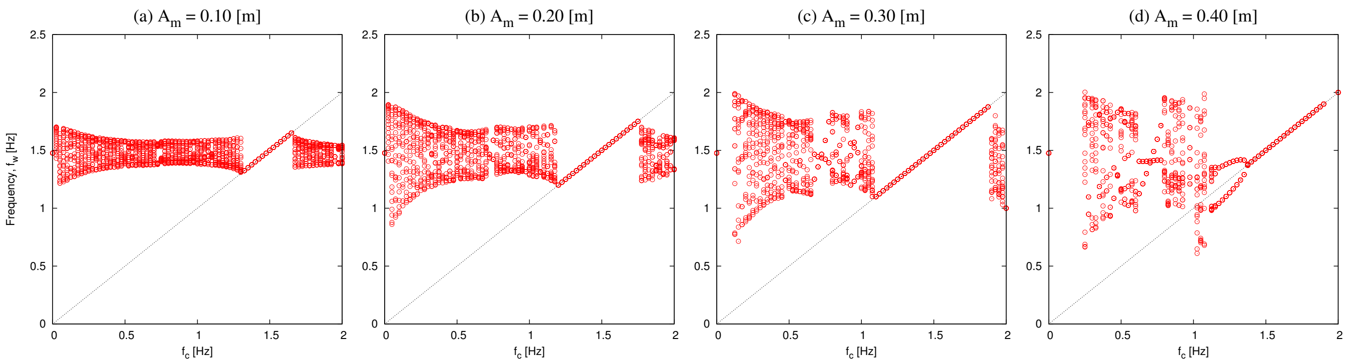

Fig. 10. Frequency of walking gait, f_w, versus desired wobble frequency, f_c, for four values of A_m where $\phi = 0.13$ [rad] and $L_0 = 0.30$ [m]

C. Analysis Results

Fig. 10 shows the analysis results of the frequency, f_w, for four values of A_m with respect to f_c. We followed the procedure 1 for gait analysis but chose the initial velocity condition as $\dot{\boldsymbol{q}}(0) = \begin{bmatrix} 0 & 0 & 1.0 & 0 & 0 \end{bmatrix}^{\mathrm{T}}$.

By focusing mainly on Fig. 10 (c), a typical transition from desynchronization to synchronization between the RW and the wobbling mass can be observed as follows [14]. For a small frequency of f_c, the RW is only weakly influenced by the wobbling mass and it oscillates with its own natural frequency of around 1.5 [Hz]. Here, the dense plots of f_w represent a sign of quasi-periodic motion. The averaged frequency of f_w, however, remains in a similar range to the natural frequency. As f_c becomes close to 1.1 [Hz], f_w shows a periodic motion, whose value coincides with f_c (f_w grows on a diagonal line of $f_w = f_c$). This indicates that the motion of the RW is entrained to the rotational movement of the wobbling mass [14]. Therefore, we can conclude that the average walking speed can be increased by choosing f_c as larger than 1.5 [Hz].

The effect of entrainment would be increased by using a heavier wobbling mass. The effects of the physical parameters, L_0, k and c, are also crucial for the gait stability. More analysis is necessary.

V. CONCLUSION AND FUTURE WORK

In this paper, we investigated the fundamental properties in passive dynamic walking of a planar RW with passive and active 2-DOF wobbling masses. Through numerical investigations, some interesting properties such as bifurcation, hysteresis, and entrainment have been observed.

As previously mentioned, identifying the dominant mode that characterizes the gait properties is left as a future work. In addition, theoretical investigations from the viewpoint of the dynamic absorber should be conducted in the future.

In the active case, we examined only the effect of rotational control. Active control of the telescopic motion is also an interesting subject to be investigated. With the progress in the above studies, proper methods for use of a 2-DOF wobbling mass would be developed.

REFERENCES

[1] D. Tanaka, F. Asano and Isao Tokuda, "Gait analysis and efficiency improvement of passive dynamic walking of combined rimless wheel with wobbling mass," *Proc. of the IEEE/RSJ Int. Conf. on Intelligent Robots and Systems*, pp. 151–156, 2012.

[2] Y. Hanazawa, T. Hayashi, M. Yamakita and F. Asano, "High-speed limit cycle walking for biped robots using active up-and-down motion control of wobbling mass," *Proc. of the IEEE/RSJ Int. Conf. on Intelligent Robots and Systems*, 2013. (to appear)

[3] F. Asano and I. Tokuda, "Gait control of passive combined rimless wheel using active wobbling mass," *Proc. of the IEEE Int. Conf. on Mechatronics and Automation*, 2013. (to appear)

[4] F. Asano, Y. Akutsu and I. Tokuda, "Gait control of combined rimless wheel using active wobbling mass that vibrates backward and forward," *Proc. of the 10th Int. Conf. on Ubiquitous Robots and Ambient Intelligence*, 2013. (to appear)

[5] C. D. Remy, K. Buffinton and R. Siegwart, "Stability analysis of passive dynamic walking of quadrupeds," *Int. J. of Robotics Research*, pp. 1173–1185, 2010.

[6] N. Maheshwari, X. Yu, M. Reis and F. Iida, "Resonance based multi-gaited robot locomotion," *Proc. of the IEEE/RSJ Int. Conf. on Intelligent Robots and Systems*, pp. 169–174, 2012.

[7] R. M. Alexander, "Breathing while trotting," *Science*, Vol. 9, No. 5131, pp. 196–197, 1993.

[8] L. C. Rome, L. Flynn, E. M. Goldman and T. D. Yoo, "Generating electricity while walking with loads," *Science*, Vol. 309, No. 5741, pp. 1725–1728, 2005.

[9] L. C. Rome, L. Flynn and T. D. Yoo, "Biomechanics: Rubber bands reduce the cost of carrying loads," *Nature*, Vol. 444, No. 7122, pp. 1023–1024, 2006.

[10] R. Inoue, F. Asano, D. Tanaka and I. Tokuda, "Passive dynamic walking of combined rimless wheel and its speeding-up by adjustment of phase difference," *Proc. of the IEEE/RSJ Int. Conf. on Intelligent Robots and Systems*, pp. 2747–2752, 2011.

[11] T. McGeer, "Passive dynamic walking," *Int. J. of Robotics Research*, Vol. 9, No. 2, pp. 62–82, 1990.

[12] M. J. Coleman, A. Chatterjee and A. Ruina, "Motions of a rimless spoked wheel: a simple three-dimensional system with impacts," *Dynamics and Stability of Systems*, Vol. 12, Issue 3, pp. 139–159, 1997.

[13] F. Asano, "Stability principle underlying passive dynamic walking of rimless wheel," *Proc. of the IEEE Int. Conf. on Control Applications*, pp. 1039–1044, 2012.

[14] A. Pikovsky, M. Rosenblum, and J. Kurths, *Synchronization - A Universal Concept in Nonlinear Sciences*, Cambridge University Press, Cambridge, 2001.